E versus Z isomers of Fischer aminocarbene complex $[Mo(CO)_4(PPh_3)\{C(NHCy)(2\text{-furyl})\}]$: N–H···O *versus* C–H···O intramolecular hydrogen bonds

Marilé Landman[a] and Jeanet Conradie[b]**

a Department of Chemistry, University of Pretoria, Private Bag X20, Hatfield, 0028, South Africa. Tel: 27-12-4202527, Fax: 27-12-4204687

b Department of Chemistry, PO Box 339, University of the Free State, Bloemfontein, 9300, South Africa. Tel: 27-51-4012194, Fax: 27-51-4017295

Contact author details:

Name: Jeanet Conradie, Tel: ++27-51-4012194, Fax: ++27-51-4017295, email: *conradj@ufs.ac.za*

Name: Marilé Landman Tel: ++27-12-4202527, Fax: ++27-12-4204687, email: *marile.landman@up.ac.za*

Keywords

Fischer carbene; Molybdenum; DFT; NBO analysis; hydrogen bond, QTAIM

Graphical abstract

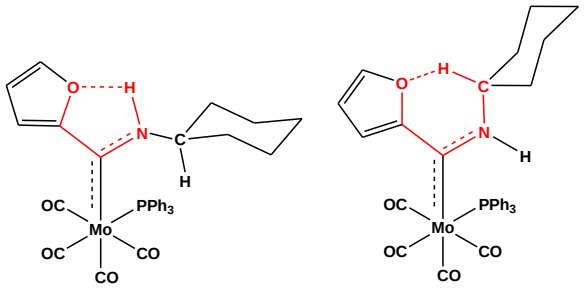

TOC abstract

X-ray, NBO and QTAIM analysis of the *E* and *Z* isomers of a Fischer Mo-aminocarbene complex

Research highlights

- DFT conformation analysis yields 12 possible structural conformations
- Crystal structure shows *syn* conformation for the two heteroatoms
- Crystal structure shows *Z* conformation for cyclohexyl group relative to Mo
- Crystal structure shows *cis* isomer for PPh_3 relative to the carbene ligand
- Calculated NBO donor-acceptor interactions show intramolecular H-bond interactions

Abstract

A density functional theory (DFT) calculated conformation analysis of the twelve possible conformations of $[Mo(CO)_4(PPh_3)\{C(NHCy)(2\text{-furyl})\}]$, **1**, utilizing different DFT methods, showed that both the *cis-syn,Z* (2), **1**-*Z*, and the *cis-syn,Z* (2), **1**- *E*, conformations of this aminocarbene complex have similar electronic and Gibbs free energies. The solid-state crystal structure of the **1**- *Z* is presented in this study and compared to the structure of the **1**- *E* conformation. The stability of **1**-*Z*, *versus* the previously published solid-state structure of conformer **1**-*E*, is ascribed to stabilization of the $N–H\cdots O_{Fu}$ intramolecular bond. This is evidenced by a shorter $H\cdots O$ intramolecular bond in the experimental crystal structure of **1**-*Z*. The stability of the **1**-*Z* and **1**- *E* conformations were analyzed and compared by density functional theory, quantum theory of atoms in molecules (QTAIM) and natural bond orbital (NBO) methods. The NBO analysis reveals similar but stronger donor-acceptor interactions in **1**-*Z* than in **1**- *E*. QTAIM calculations indicate 6 and 5 bond critical points related to intramolecular bonds stabilizing the orientation of 2-furyl and NHCy in **1**-*Z* and **1**- *E* respectively.

1 Introduction

Since the discovery of the first Fischer carbene complex, $[(CO)_5W=C(Ph)(OMe)]$ [1], many Fischer-type carbene complexes have been synthesized and tested for their catalytic properties,

mainly in organic synthesis [2]. Isomerism in Fischer carbene complexes has been shown to influence the reactivity and final product formation in reactions with the different isomers [3]. For instance, two isomeric chiral ligand-modified molybdenum and chromium Fischer carbene complexes, *fac* and *mer*, were shown to yield different diastereoselectivities towards acrylonitrile in cyclopropanation reactions [4]. The use of Fischer carbene complexes in transition metal catalyzed processes has met with some difficulty in the past [5]. This can be ascribed to the relative high stability of the Fischer carbene complex. Fischer carbene complexes are electrophilic at the carbene carbon, and the low oxidation state of the metal ion is often stabilized by a heteroatom X, where X = N, O, or S. Due to the lone-pair electrons of the heteroatom, bond delocalization between M-$C_{carbene}$ and X-$C_{carbene}$ occurs; see Scheme 1 (a). Carbene complexes containing an amino substituent can exhibit either an *E* or a *Z* configuration [6] due to restricted rotation around the $C_{carbene}$–N bond, which has partial double bond character due to π-donation from the nitrogen atom to the carbene carbon [7], as illustrated in Scheme 1. The assignment of *E* or *Z* is determined by the relative positions of the two higher priority substituents (R and H in Scheme 1 (b)) about the $C_{carbene}$–N "double bond" according to the Cahn-Ingold-Prelog priority rules (higher atomic numbers have higher priority). Licandro *et al.* [8] was able to isolate both *E* and *Z* isomers of a pentacarbonyl methyl(hydrazino)carbene complex of chromium(0) using flash chromatography and reported the crystal structures of both isomers. The two isomers displayed different reactivities, which could be explained by their different structural features. The solid-state structure of the *E* isomer of $[Mo(CO)_4(PPh_3)\{C(NHCy)(2\text{-furyl})\}]$, **1**, has recently been reported by us [9]. The solid-state structure of the *Z* isomer of **1** is presented here and compared to the previously published solid-state structure of the *E* isomer in order to investigate structural differences between the two configurations with the aid of theoretical calculations.

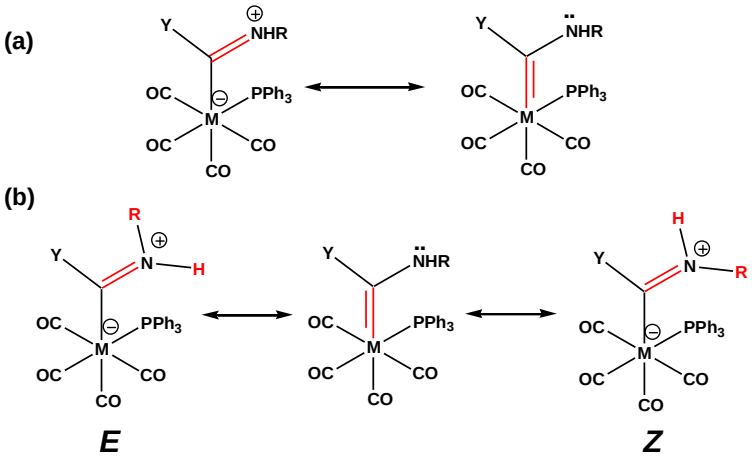

Scheme 1. (a) Lone pair electron bond delocalisation and (b) *E* and *Z* isomers of aminocarbene complexes with amino group NHR (R = alkyl or aryl)

2 Experimental

2.1 Synthesis of $[Mo(CO)_4(PPh_3)\{C(NC_6H_{12})(C_4H_3O)\}]$, 1

The title complex was synthesized as described in literature [9]. Experimental and characterization data are presented for completeness. All reactions, unless otherwise noted, were performed under inert nitrogen or argon atmospheres using standard Schlenk techniques [10]. All solvents were freshly distilled, dried and collected under inert conditions, with the exception of toluene. Toluene was not dried, but used after bubbling nitrogen gas through the solvent for 5 to 10 minutes. Column chromatography was carried out under inert nitrogen and argon atmospheres using silica gel (particle size 0.063-0.200 mm) as the stationary phase. Percentage yields were calculated relative to the limiting reactant. Triethyloxonium tetrafluoroborate [11] was prepared according to a reported literature procedure. The reagents $[Mo(CO)_6]$, *n*-butyl lithium (1.6 M solution in hexane), furan, PPh_3, cyclohexyl amine (NH_2Cy) and other commercial reagents were used as purchased. $[Mo(CO)_5\{C(NC_6H_{12})(C_4H_3O)\}]$ was synthesized as reported in literature [9]. NMR spectra were recorded on a Bruker ARX-300. NMR spectra were recorded in C_6D_6 and $CDCl_3$ using deuterated solvent peaks as the internal references. ^1H, ^{13}C and ^{31}P NMR spectra were measured at 300.1, 75.5 and 81 MHz, respectively. IR spectra were recorded on a Perkin Elmer Spectrum RXI FT-IR spectrophotometer as KBr pellets and only the vibration bands in the carbonyl-stretching region (*ca.* 1500-2200 cm^{-1}) are reported. Mass spectra were recorded on a

SYNAPT G2 HDMS with the TOF-MS method with sampling time of 4 minutes, with direct infusion inlet method. The source was electron spray ionization.

Triphenylphosphine (0.39 g, 1.5 mmol) was dissolved in 20 ml toluene. $[Mo(CO)_5\{C(NC_6H_{12})(C_4H_3O)\}]$, (0.41 g, 0.99 mmol) was dissolved in toluene and added to the triphenylphosphine solution. This was reacted under reflux for two hours and the solvent was removed. The solution mixture went from yellow to a very dark colour. Purification using silica gel column chromatography (eluent hexane:DCM gradients) yielded the product. (Yield 0.276 g; 43%).

IR (KBr; cm^{-1}): ν_{CO} 2006 (w), 1887 (s). ^{1}H NMR (δ/ppm in C_6D_6): 8.62 (s, N**H**, *E*-isomer), 8.71 (s, N**H**, *Z*-isomer), n.o (H10), 6.70 (s, H8), 5.77 (dd, H9, J = 1.8, 3.6 Hz), 4.53 (m, CHCy), 1.15-1.80 (m, Cy), 7.40-7.65 (m, P**Ph$_3$**). ^{1}H NMR (δ/ppm in $CDCl_3$): 8.74 (s, N**H**, *E*-isomer), 8.71 (s, N**H**, *Z*-isomer), n.o (H10), 6.81 (dd, H8, J = 3.6 Hz), 6.19 (dd, H9, J = 1.8, 3.6 Hz), 4.30 (m, CHCy), 1.21-1.76 (m, Cy), 7.27-7.37 (m, P**Ph$_3$**). ^{13}C NMR (δ/ppm in C_6D_6): 238.6 (C6), 218.8 (CO1), 214.6 (CO3), 211.7 (CO2, CO4), 159.1 (C7), 126.5 (C8), 113.4 (C9), 144.0 (C10), 66.2 (**C**HCy), 33.5, 25.6, 25.0 (Cy), 128.5-137.0 (P**Ph$_3$**). ^{31}P NMR (δ/ppm in C_6D_6): 40.49 (**P**Ph$_3$). ^{31}P NMR (δ/ppm in $CDCl_3$): 39.720 (**P**Ph$_3$) Anal. Calcd: C, 61.21; H, 4.67; N, 2.16. Found: C, 61.26; H, 4.36; N, 1.77.

A sample from this complex was divided into two batches. One batch was dissolved in a dichloromethane:hexane (1:1) solution while the other batch was dissolved in benzene. The crystals of **1**-*E* was formed from the benzene solution [9] while crystals of **1**-*Z* was yielded from the dichloromethane:hexane solution.

2.2 DFT calculations

Density functional theory (DFT) calculations of this study were performed with the PW91 [12], B3LYP [13,14] and the M06 [15] functionals as implemented in the Gaussian 09 program package [16]. Geometries of the neutral complexes were optimized with the def2-TZVPP or the dev2-SVP basis set [17] on Mo and 6-311G(d,p) on the other atoms. Geometries were optimized in the gas phase and selected calculations were done taking solvent effects into account. Solvation effects were computed by performing full geometry optimizations with the IEFPCM model, using benzene (ε = 2.3), hexane (ε = 1.88) or dichloromethane (ε = 8.9) as solvent. Geometries obtained by gas phase calculations (B3LYP, PW91 and M06) for the different conformations were confirmed as true minima in the potential energy surface by computation of

vibrational frequencies (no imaginary frequencies). The natural bond orbital (NBO) calculations were done on the gas phase B3LYP optimized structures, on the same level of theory, using the NBO 3.1 module [18] in Gaussian 09. The topological analysis of the electron charge density performed for the complexes was determined using Bader's quantum theory of atoms in molecules (QTAIM) [19] on the gas phase B3LYP optimized structures. The electronic density analysis was performed using QTAIM [20] as implemented in ADF2013 [21] at the same level of theory.

2.3 X-ray Crystallography

Crystals suitable for single crystal X-ray crystallography were obtained by recrystallization from a dichloromethane:hexane (1:1) solution. Crystal data for **1-*Z*** was collected at 150(2) K on a Bruker D8 Venture kappa geometry diffractometer with duo Iμs sources, a Photon 100 CMOS detector and APEX II [22] control software using Quazar multi-layer optics monochromated, Mo-*K*α radiation by means of a combination of ϕ and ω scans. Data reduction was performed using SAINT+ [22] and the intensities were corrected for absorption using SADABS [22]. The structure was solved by intrinsic phasing using SHELXTS [23] and refined by full-matrix least squares using SHELXTL and SHELXL-97/2013/2014 [23]. In the structure refinement, all hydrogen atoms attached to carbon atoms were added in calculated positions and treated as riding on the atom to which they are attached. All non-hydrogen atoms were refined with anisotropic displacement parameters, all isotropic displacement parameters for hydrogen atoms were calculated as X × Ueq of the atom to which they are attached, X = 1.5 for the methyl hydrogens and 1.2 for all other hydrogens. Crystal data, data collection, structure solution and refinement details are available in the CIF (CCDC 1048219). An Ortep drawing [24] of the structure is given in Figure 1(a), showing the numbering system used with ADP's at the 50% probability level. Crystallographic data is included in Table 1.

3 Results and Discussion

3.1 Synthesis and characterization

Different conformations are possible for the aminocarbene complex $[Mo(CO)_4(PPh_3)\{C(NHCy)(2\text{-furyl})\}]$, **1**. Firstly, the oxygen atom of the 2-furyl ring in **1** can be orientated on the same side than the NHCy substituent (*syn* conformation) or have the opposite orientation (*anti* conformation). Furthermore, the NHCy group in **1** can adopt either an *E* or Z orientation relative to Mo, leading to four possible conformers: *syn,Z*; *anti,Z*; *syn,E* and *anti,E*. If the PPh_3 group in **1** is in the *cis* position relative to the carbene ligand, it can be either nearest to the furyl ring or nearest to the NHCy, leading to eight possible *cis*-PPh_3 conformers for **1**. If the PPh_3 is in the *trans* position, four *trans*-PPh_3 conformers are possible. The twelve different conformations of **1** are shown in Scheme 2.

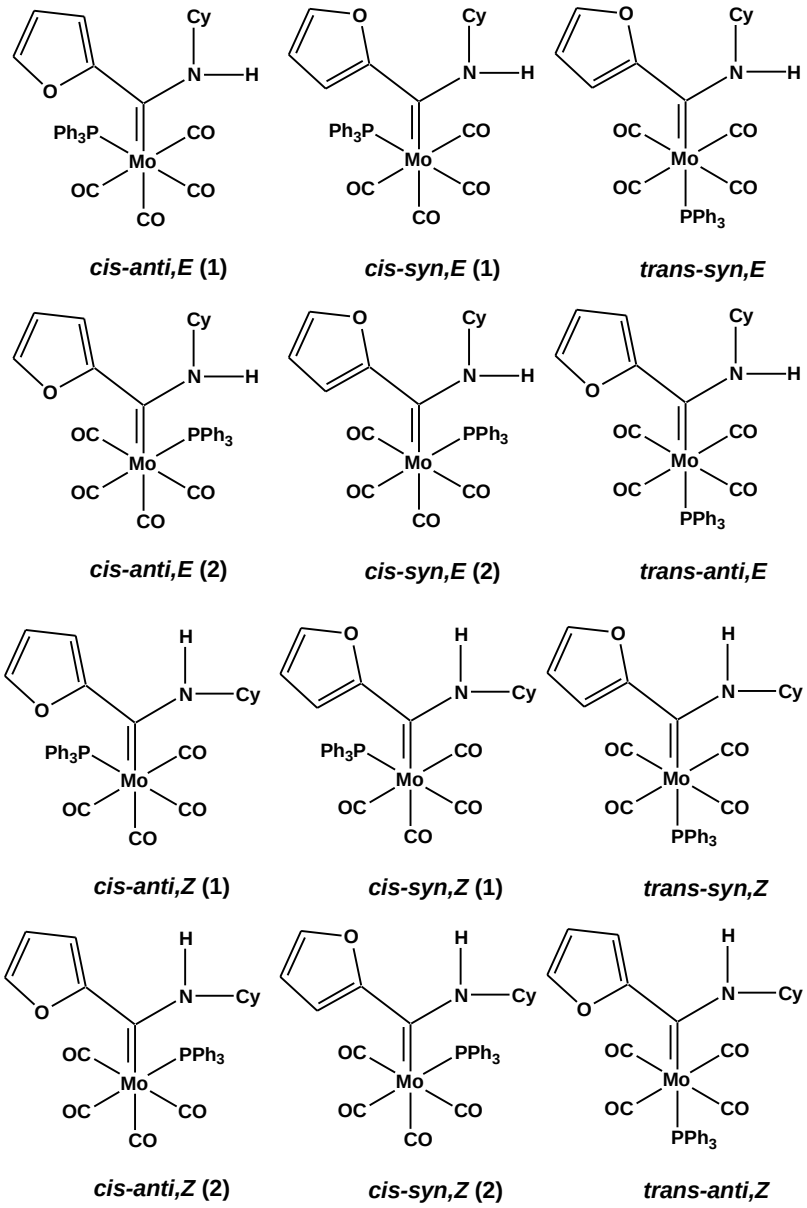

Scheme 2. The twelve different conformations possible for **1**

The synthesis of **1** has been described previously [9]. Incorporation of phosphines into the Fischer carbene complex's ligand sphere can either be achieved before introduction of the carbene ligand, in employing $[M(CO)_5PR_3]$ during the classical Fischer synthesis, or after. The latter method entails normal carbonyl substitution methods of the ethoxy carbene, i.e. thermal or photolytic substitution [25,26]. In the first case, *cis*-substituted tetracarbonyl phosphine carbene complexes are formed almost exclusively [25b,e], while in the latter case a mixture of both the *cis* and *trans* isomers is obtained. However, literature reports favour the *cis*-substituted complex

as having higher stability than the *trans* complex due to electronic considerations [26]. In fact, to date only one *trans* complex could be structurally characterized, namely the *trans*-[$(CO)_4(PPh_3)W=C(OEt)(2\text{-furyl})$] [27] complex. Furthermore, phosphine ligand substitution can precede or follow aminolysis [28] of the ethoxy carbene complex. The latter reaction order is associated with a distinctive colour change from the yellow pentacarbonyl aminocarbene complex to the red phosphine-substituted aminocarbene product [9]. On the proton NMR spectra of the complex in either C_6D_6 or $CDCl_3$ as solvent, both isomers are present in a 1:1 (*E*:*Z*) ratio.

3.2 Crystallographic structure

The crystal structure of the *cis-syn,Z* (2) conformer of **1** presented in this study is shown in Figure 1. Crystallographic and refinement data can be found in Table 1. Selected structural parameters of importance are summarized in Table 2. Previously published structural data of the *cis-syn,E* (2) conformer of **1** [9] is added to Table 2 for comparative purposes**.**

PPh_3 position: Crystal structures of sixteen Fischer carbene complexes of the formula [$(CO)_4(PPh_3)M=C(X)Y$] have been reported to date [9,26,27,29], with only one structure having the PPh_3 group *trans* to the carbene ligand, namely the [$(CO)_4(PPh_3)W=C(OEt)(2\text{-furyl})$] [27] complex. In all the other structures, the *cis*-isomer was characterized, similar to the structure of **1**.

Furyl ring orientation: The crystal structures of nine Fischer aminocarbene complexes of the formula [$(CO)_3LL'M=C(NHR)(2\text{-furyl})$] all have the 2-furyl ring in the *syn* conformation [9,30], similar to **1**. By contrast, most of the corresponding alkoxy carbene complexes exhibit the *anti* conformation [9,26,30c,31].

***E* / *Z* conformation**: The *E* isomer of **1** has been characterized structurally recently [9]. However, the unit cell included a molecule of benzene solvent. The only additional structure with formula [$(CO)_4(PPh_3)M=C(NHR)X$] reported to date, is [$(CO)_4(PPh_3)W=C(NHCy)(2\text{-thienyl})$] [31b]. In this structure, the *Z* isomer is observed, similar to the preferred structure of **1**, the structure shown in **Figure 1**.

Hydrogen bonding: In the solid-state structures of four related Mo-aminocarbene complexes containing a furyl group, hydrogen bonding (O…H-N) between the O_{Fu} and the H of the amino-group ranges from 2.125 Å - 2.267 Å [9]. The N1-H…O6 hydrogen bond of 2.109 Å in the *Z*

isomer of **1** is shorter than the hydrogen bond in the related structures and also shorter than the hydrogen bond between C11-H…O6 of 2.346 Å in the *E* isomer of **1**.

The other bond lengths and angles are very similar in the *E* and *Z* structures of **1**, as shown in Table 2. The only noticeable exception is the Mo1-C6-N1 bond angle. Due to the stronger, shorter N1-H…O6 hydrogen bond, this angle is larger for the *Z* isomer (128.36(12)°) than for the *E* isomer (116.3(3)°), where the C11-H…O6 hydrogen bond interaction is weaker.

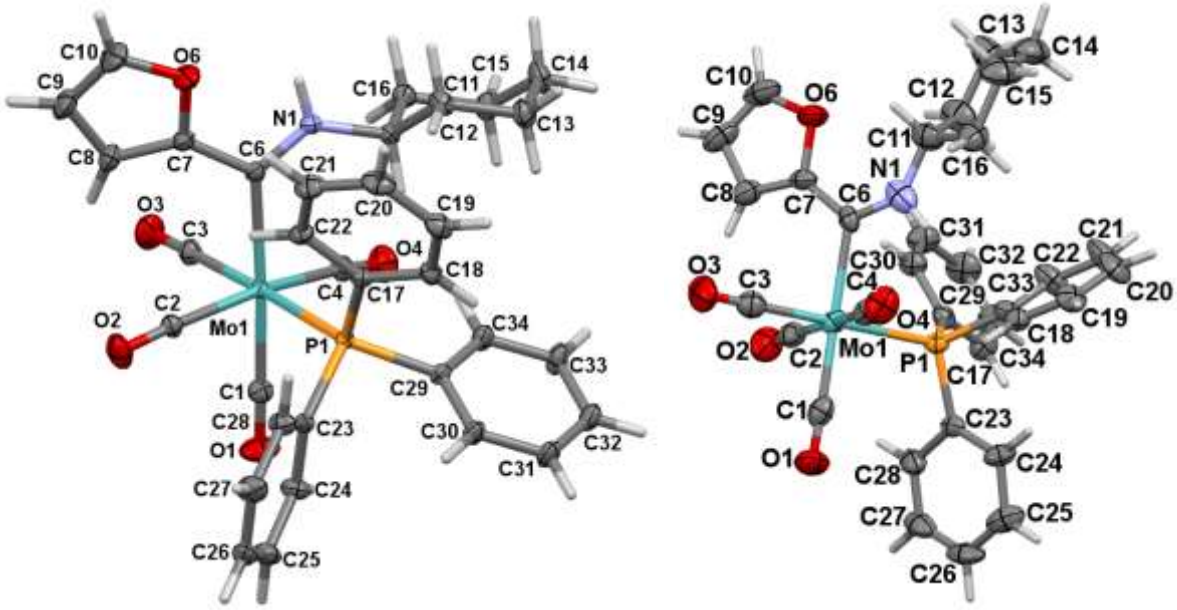

Figure 1. Perspective views of the (a) *cis-syn,Z* (2) and (b) *cis-syn,E* (2) [9] conformers of **1** with thermal ellipsoids drawn at the 50% probability level.

The N1-C6-C7 bond angle differs quite significantly in the two structures, *ca.* 10°. This is attributed to the formation of a five-membered ring system (**1**-*Z*) and a six-membered ring system (**1**-*E*), respectively, through hydrogen bonding (see Figure 2). Therefore **1**-*Z* will have a smaller bond angle for N1-C6-C7.

Table 1. Crystallographic and refinement data for **1**-*Z*

Empirical formula	$C_{33}\ H_{30}\ Mo\ N\ O_5\ P$
Formula weight (g mol^{-1})	647.49
Temperature (K)	150(2)
Radiation type, λ (Å)	Mo Kα, 0.71073
Crystal system, space group	Monoclinic, C c
a (Å)	18.238(2)
b (Å)	15.2729(17)
c (Å)	10.7617(13)
β (°)	93.154(4)
Volume ($Å^3$)	2993.1(6)
Z, D_{calc} (Mg/m^3)	4, 1.437
Absorption coefficient (mm^{-1})	0.533
F(000)	1328
Crystal size (mm^3)	0.704 x 0.496 x 0.224
Theta range for data collection (°)	2.528 to 45.738
Index ranges	$-36\leq h\leq 36$, $-30\leq k\leq 30$, $-21\leq l\leq 21$
Reflections collected	219253
R(int)	0.0976
Absorption correction	Semi-empirical from equivalents
Max. and min. transmission	0.7489 and 0.5923
Refinement method	Full-matrix least-squares on F^2
Data used / restraints / parameters	25504 / 2 / 370
Goodness-of-fit on F^2	1.024
Final R indices [I>2sigma(I)]	R1 = 0.0420, wR2 = 0.0756
Largest diff. peak and hole ($e.Å^{-3}$)	1.599, -0.476

Table 2. Selected geometric parameters for the *cis-syn,Z* (2) and *cis-syn,E* (2) [9] conformers of **1**

$[Mo(CO)_4(PPh_3)\{C(NHCy)(2\text{-furyl})\}]$, **1**		
Conformer	*cis-syn,Z* (2)	*cis-syn,E* (2)[a] [9]
Bond length (Å)		
Mo1-$C6_{carbene}$	2.2693(17)	2.257(4)
Mo1-C1	1.9870(19)	2.001(5)
Mo1-C2	2.0293(19)	2.028(5)
Mo1-C4	2.0285(18)	2.027(5)
Mo1-C3 (*trans* to P)	1.9812(18)	1.978(5)
Mo1-P1	2.5669(5)	2.557(1)
C6-N1	1.310(2)	1.324(6)
C6-C7	1.465(2)	1.439(6)
Bond angle (°)		
Mo1-C6-N1	128.36(12)	116.3(3)
Mo1-C6-C7	120.90(12)	122.1(3)
N1-C6-C7	110.73(15)	120.9(4)
Torsion angle (°)		
N1-C6-C7-O6	-14.5(2)	1.5(6)
Mo1-C6-C7-O6	165.15(14)	177.3(3)

[a] Structure includes benzene solvent molecule in unit cell

3.3 DFT study

Results of a density functional theory (DFT) computational chemistry study recently presented by us [9], utilizing the B3LYP functional, showed that the small difference in the DFT calculated electronic energy between some of the conformers of the same Fischer Mo carbene complex indicates that more than one conformer should be experimentally feasible. **Table 3** gives the relative electronic and Gibbs free energies obtained for the twelve different conformations of **1** utilizing different DFT methods. For **1** the conformer with the lowest DFT calculated gas phase electronic energy, obtained by all three functional used (B3LYP, PW91 and M06), is the *cis-syn,Z* (2) conformer (conformer 11), the conformer of which the solid-state crystal structure is presented in this study. The corresponding *E* isomer, the *cis-syn,E* (2) (conformer 12), of which the solid-state crystal structure has previously been published [9], is between 0.7 – 13.1 kJ mol^{-1} higher in energy, depending on the functional used. The electronic energy ordering of the

conformers does not change significantly when solvent effects (hexane, benzene or dichloromethane) were taken into account in the calculations; conformers *cis-syn,Z* (1) (conformer 7), *cis-syn,Z* (2) (conformer 11) and *cis-syn,E* (2) (conformer 12) (Scheme 2, **Table 3**) are near equi-energetic, and all should thus be experimentally feasible. When considering the Gibbs energy ordering of the conformers, we observe that conformers *cis-syn,Z* (1) (conformer 7), *cis-syn,Z* (2) (conformer 11) and *cis-syn,E* (2) (conformer 12) are under the four lowest energy conformers for all functionals (B3LYP, PW91 and M06) used. However, the small energy differences obtained between most of the conformers could be considered as equi-energetic within the accuracy of DFT [32]. The fact that we were able to experimentally isolate another isomer of **1**, is thus in agreement with the DFT results. Results of DFT calculations to further evaluate the stability of the two conformers of **1** experimentally isolated in the solid state, *cis-syn,Z* (2) (conformer 11) and *cis-syn,E* (2) (conformer 12), are thus presented.

Table 3. DFT-calculated electronic and Gibbs free energies for possible conformers of **1**, calculated with different computational methods. See Scheme 2 for the structures of the different conformers.

Conformer	Relative electronic energy / kJ mol^{-1}							Relative Gibbs free energy / kJ mol^{-1}		
	B3LYP gas phase[a,b]	B3LYP benzene[a,b,c]	B3LYP benzene + 1 benzene[a,b,c]	B3LYP DCM[b,c,d]	B3LYP hexane[b,c]	M06 gas phase[b]	PW91 gas phase[e]	B3LYP gas phase[b]	M06 gas phase[b]	PW91 gas phase[e]
trans-anti,Z	18.40	19.55	25.13	20.50	19.33	41.31	21.88	14.03	40.66	16.68
trans-anti,E	25.06	25.25	30.96	26.29	25.13	57.55	29.63	15.10	49.12	19.07
trans-syn,Z	7.53	10.23	15.35	12.93	9.67	30.28	10.56	2.27	28.70	6.78
trans-syn,E	19.45	21.09	26.60	23.52	20.66	54.40	24.20	9.38	35.57	14.51
cis-anti,Z (1)	8.19	6.68	9.74	4.54	7.03	10.38	11.19	5.58	17.32	9.79
cis-anti,E (1)	14.34	10.95	16.24	8.34	11.53	25.29	17.82	8.47	26.83	13.13
cis-syn,Z (1)	0.001	0.00	0.00	0.00	0.00	4.98	1.28	0.54	13.86	1.74
cis-syn,E (1)	10.88	9.41	9.26	8.57	9.66	26.17	13.76	4.29	16.02	8.98
cis-anti,Z (2)	13.61	12.23	13.26	10.34	12.52	16.41	10.18	14.24	18.13	14.68
cis-anti,E (2)	11.53	9.02	9.75	7.00	9.50	26.63	13.48	10.23	25.69	15.00
cis-syn,Z (2)	0.000	0.21	3.75	0.76	0.13	0.00	0.00	3.40	0.00	3.60
cis-syn,E (2)	0.70	0.02	3.27	0.40	0.08	13.07	2.02	0.00	10.18	0.00

[a] Data from [9].
[b] Basis set: 6-311G(d,p) on all atoms except Mo, where def2-TZVPP was used
[c] Implicit solvent model
[d] DCM = dichloromethane
[e] Basis set: 6-311G(d,p) on all atoms except Mo, where def2-SVP was used

The orientation of NHCy with respect to Mo in the *cis-syn,Z* (2) and the *cis-syn,E* (2) conformers of **1** leads respectively to the formation of a five- and six membered chelate ring due to the intramolecular hydrogen bonds, see Scheme 3. In *cis-syn,Z* (2) the B3LYP gas phase DFT calculated N–H…O_{Fu} bond is 2.059 Å (2.109 Å experimental value). In *cis-syn,E* (2) the DFT calculated C–H…O_{Fu} is 2.250 Å (2.346 Å experimental value). These hydrogen bonds can be categorized as medium (1.5-2.2 Å) to weak (2.2-3.2 Å) [33,34]. The hydrogen bonds in *cis-syn,Z* (2) and *cis-syn,E* (2) conform also to another commonly used method for identifying hydrogen bond interactions, namely that distances between the donor and acceptor groups equal or less than that of the sum of the atoms' van der Waals radii are indicative of hydrogen bond formation [35], *viz* d(H…O) = 2.7 Å for the bonds mentioned above [36]. The N–H…O_{Fu} hydrogen bond in *cis-syn,Z* (2) is shorter and stronger than the C–H…O_{Fu} bond in *cis-syn,E* (2). The similarity of the B3LYP gas phase DFT calculated hydrogen bond angles (θ indicated in Scheme 3) of 109.2° (*Z*) and 110.9° (*E*) indicates that the bond is not subjected to more strain in the five-membered than in the six-membered chelate ring, see Figure 2. These experimental values are 113.54° (*Z*) and 110.7° (*E*), respectively.

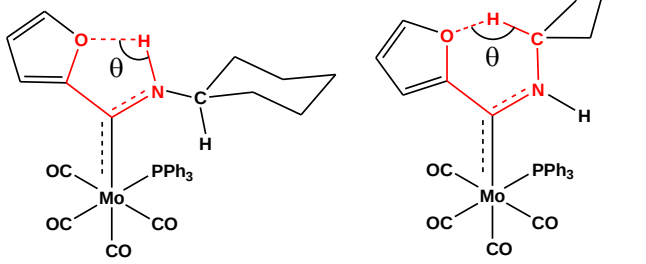

cis-syn,Z (2) ***cis-syn,E (2)***

Scheme 3. Hydrogen-bond formation in *E* and *Z* isomers of the Fischer aminocarbene $[Mo(CO)_4(PPh_3)\{C(NHCy)(2\text{-furyl})\}]$, **1**

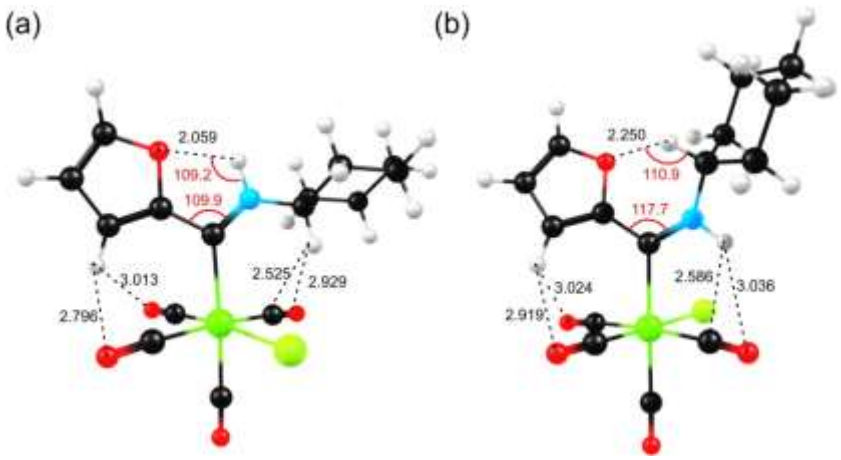

Figure 2. Selected intramolecular geometrical donor-acceptor distances (Å) and angles (°) in the B3LYP gas phase DFT optimized structure of (a) *cis-syn,Z* (2) and (b) *cis-syn,E* (2). Ph-rings are removed for clarity. Colour code of atoms (online version): Mo (green), C (black), P (lime green), O (red), N (blue), H (white).

An NBO analysis of the *cis-syn,Z* (2) and the *cis-syn,E* (2) conformers of **1** reveals the following (data in **Table 4**):

i) a conjugative interaction between a O_{Fu} lone pair (LP) and the antibonding orbital (BD*) of the N–H bond, LP1(O) → BD*(N–H) of 5.7 kJ mol^{-1} for *cis-syn,Z* (2) (see Figure 3(a1)), and

ii) a much weaker (< 0.2 kJ mol^{-1}) conjugative interaction between a O_{Fu} lone pair (LP) and the antibonding orbital (BD*) of the C–H bond, LP1(O) → BD*(C–H), for *cis-syn,E* (2) (see Figure 3(b1)).

The NBO analysis further shows that the carbene ligand in *cis-syn,E* (2) is also stabilized by donor-acceptor interactions between the π-bonding orbital on a CO and the antibonding orbital (BD*) of the N–H bond (Figure 3(b3)), as well as the π-bonding orbital on another CO and the antibonding orbital (BD*) of a furyl ring C–H bond (Figure 3(b2)). Similar, but weaker, donor-acceptor interactions exist for *cis-syn,Z* (2); see Figure 3(a3) and (a2) and **Table 4**.

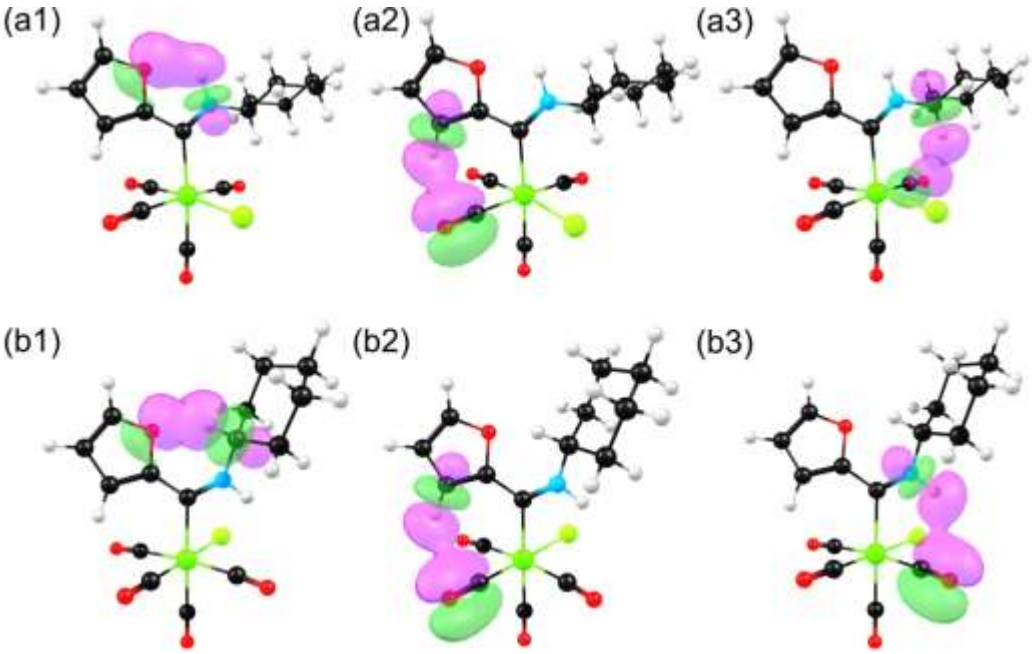

Figure 3. NBO analysis donor-acceptor interaction in B3LYP gas phase DFT optimized structure of (a) *cis-syn,Z* (2) and (b) *cis-syn,E* (2). Ph-rings are removed for clarity. The NBO plots use a contour of 60 e/nm^3. Colour code of atoms (online version): Mo (green), C (black), P (lime green), O (red), N (blue), H (white).

The donor-acceptor NBO calculated interactions (> 0.2 kJ mol^{-1}) related to the orientation of the NHCy group in *cis-syn,Z* (2) and *cis-syn,E* (2), in order of bond energy strength (**Table 4**) are:

(i) LP1(O) → BD*(N1–H1) (5.7 kJ mol^{-1}) in *cis-syn,Z* (2) (Figure 3(a1))

(ii) BD(C18–C19)$_{\text{Ph ring}}$ → BD*(N1–H1) (0.33 kJ mol^{-1}) in *cis-syn,E* (2) (not shown in Figure 3)

(iii) BD(O3–C3)$_{\text{CO group}}$ → BD*(C8–H8) (0.29 kJ mol^{-1}) in *cis-syn,E* (2) (Figure 3(b2))

(iv) BD(O4–C4)$_{\text{CO group}}$ → BD*(N1–H1) (0.21 kJ mol^{-1}) in *cis-syn,E* (2) (Figure 3(b3))

(v) BD(C17–C22)$_{\text{Ph ring}}$ → BD*(N1–H1) (0.21 kJ mol^{-1}) in *cis-syn,E* (2) (not shown in Figure 3).

The *Z* configuration of **1** is thus stabilized by mainly one strong donor-acceptor interaction, numbered (i) above, while the *E* configuration of **1** is stabilized by four much weaker donor-acceptor interactions, (ii) – (v) above.

Table 4. Energies of selected NBO interactions calculated for the indicated conformers of **1**

***cis-syn,Z* (2)**[a]					
LP1(O6) → BD*(N1–H1)		BD(C2–O2) → BD*(C8–H8)		BD(C4–O4) → BD*(C11–H11)	
E(2) / kJmol^{-1}	5.73		< 0.2		< 0.2
occupancy LP/BD / e	-1.968		-1.994		-1.995
occupancy BD* / e	-0.041		-0.013		-0.024
d(N–H) / Å	1.018	d(C–H) / Å	1.075	d(C–H) / Å	1.089
d(N–H…O_{Fu}) / Å	2.059	d(C–H…O_{CO}) / Å	2.796	d(C–H…O_{CO}) / Å	2.929
angle(N–H-O_{Fu}) / °	109.2	angle(C–H-O_{CO}) / °	118.8	angle(C–H-O_{CO}) / °	120.9
***cis-syn,E* (2)**[a,b]					
LP1(O6) → BD*(C11–H12)		BD(O3–C3) → BD*(C8–H8)		BD(O4–C4) → BD*(N1–H1)	
E(2) / kJ mol^{-1}	< 0.2		0.29		0.21
occupancy LP/BD / e	-1.970		-1.995		-1.994
occupancy BD* / e	-0.024		-0.012		-0.027
d(C–H) / Å	1.089	d(C–H) / Å	1.075	d(N–H) / Å	1.013
d(C–H…O_{Fu}) / Å	2.250	d(C–H…O_{CO}) / Å	2.919	d(N–H…O_{CO}) / Å	3.036
angle(C–H-O_{Fu}) / °	110.9	angle(C–H-O_{CO}) / °	127.9	angle(N–H-O_{CO}) / °	124.8

[a] Atom numbering according to Figure 1

[b] Interactions between the antibonding orbital on NH and (C-C) bonding orbitals of a phenyl ring of PPh_3 calculated is BD(C17–C22) → BD*(N1–H1) (0.21 kJ mol^{-1}) and BD(C18–C19) → BD*(N1–H1) (0.33 kJ mol^{-1})

The observed hydrogen bonds were further analyzed using Bader's quantum theory of atoms in molecules (QTAIM) theory on the B3LYP gas phase optimized geometries of *cis-syn,Z* (2) and *cis-syn,E* (2), see Figure 4. The topological analysis of the charge density ρ(r) distribution and properties of critical points (CPs) determined by QTAIM, provide an unambiguous definition of chemical bonding [37]. For *cis-syn,Z* (2) 86 bond critical points were determined, 10 of which are intramolecular bonds, two involving the 2-furyl ring, four involving the cyclohexyl amino substituent, and four involving stabilization of the phenyl rings of PPh_3. For *cis-syn,E* (2) 83 bond critical points were determined, 8 of which are intramolecular bonds, three involving the 2-furyl and five involving stabilization of the phenyl rings of PPh_3.

Table 5 summarizes selected topological parameters of the hydrogen bonds and the chelate rings in *cis-syn,Z* (2) and *cis-syn,E* (2). Focusing on bond paths and bond critical points related to the orientation of furyl and the NHCy group in *cis-syn,Z* (2) and *cis-syn,E* (2), we observe the following:

Stabilization of *syn* orientation of furyl ring: The *syn* orientation of the furyl ring in both *cis-syn,Z* (2) and *cis-syn,E* (2) is stabilized by

(a) an intramolecular N–H· · ·O_{Fu} hydrogen bond in *cis-syn,Z* (2) (see a1 in Figure 4) and a similar six-membered chelate ring in *cis-syn,E* (2) (see b1 in Figure 4). Comparing the electron density (ρ) and the Laplacian of the electron density ($\nabla^2\rho$) at the H· · ·O bond critical point of the N–H· · ·O_{Fu} hydrogen in *cis-syn,Z* (2) (0.0221 e a_0^{-3} and 0.1144 e a_0^{-5}) with that of the C–H· · ·O_{Fu} hydrogen bond in *cis-syn,E* (2) (0.0167 e a_0^{-3} and 0.0690 e a_0^{-5}), we observe that the former is larger, indicative of a stronger hydrogen bond in *cis-syn,Z* (2). This is in agreement with the shorter intramolecular distance N–H· · ·O_{Fu} in *cis-syn,Z* (2) *vs.* the intramolecular distance C–H· · ·O_{Fu} in *cis-syn,E* (2);

(b) bond path(s) running between H_{Fu} and C_{CO}, indicated by a2 and b2 for *cis-syn,Z* (2) and *cis-syn,E* (2) respectively in Figure 4. In *cis-syn,Z* (2) only one bond path with larger ρ and $\nabla^2\rho$ is obtained (a2, 0.0089 e a_0^{-3}; 0.0323 e a_0^{-5}), while in *cis-syn,E* (2) two slightly weaker bond paths (b2, 0.0075 and 0.0074 e a_0^{-3}; 0.0275 and 0.0250 e a_0^{-5}) are obtained. The topological parameters are in accordance with the DFT optimized intramolecular distances d(H_{Fu}-C_{CO}) of the interacting atoms related to the hydrogen-bonds; the parameters becoming smaller as the distance increases (distances not shown in Figure 2): 2.614 Å (H8-C2 in *Z*) < 2.717 Å (H8-C3 in *E*) < 2.765 Å (H8-C2 in *E*) < 2.791 Å (H8-C3 in *Z*, no bond path identified).

Five- *versus* six-membered chelate ring: The QTAIM results indicate the formation of a five-membered chelate ring built up by an intramolecular N–H· · ·O_{Fu} hydrogen bond in *cis-syn,Z* (2) (a1 in Figure 4) and a similar six-membered chelate ring in *cis-syn,E* (2) (b1 in Figure 4). The topological parameters (ρ and $\nabla^2\rho$) of the ring critical point of the chelate rings indicate that ρ and $\nabla^2\rho$ decrease in going from the five-membered chelate ring in *cis-syn,Z* (2) (0.0218 e a_0^{-3}; 0.1311 e a_0^{-5}) to the six-membered chelate ring in *cis-syn,E* (2) (0.0119 e a_0^{-3}; 0.0690 e a_0^{-5}).

***E* versus *Z* orientation of NHCy group**:

The Z orientation of the NHCy group in *cis-syn,Z* (2) is stabilized by the N–H· · ·O_{Fu} hydrogen bond (0.0221 e a_0^{-3} and 0.1144 e a_0^{-5}, a1 in Figure 4), the bond paths between $H11_{Cy}$ and C_{CO} (0.0109 e a_0^{-3}; 0.0332 e a_0^{-5}, a3 in Figure 4) and between $H11_{Cy}$ and C_{Ph} (0.0041 e a_0^{-3}; 0.0132 e

a_0^{-5}, a3 in Figure 4). The electron density (ρ) and the Laplacian of the electron density ($\nabla^2\rho$) of the corresponding hydrogen bond critical points in *cis-syn,E* (2) is smaller; C–H· · ·O_{Fu} hydrogen bond (0.0167 e a_0^{-3} and 0.0690 e a_0^{-5}, b1 in Figure 4) and $H1_{NH}$ and C_{Ph} (0.0050 e a_0^{-3}; 0.0167 e a_0^{-5}, b3 in Figure 4). The cyclohexyl group is additionally stabilized by two bond paths in *cis-syn,Z* (2) {between $H16_{Cy}$ and C_{CO} (0.0057 e a_0^{-3}; 0.0232 e a_0^{-5}, a4 in Figure 4) and between $H13_{Cy}$ and C_{Ph} (0.0045 e a_0^{-3}; 0.0144 e a_0^{-5}, a4 in Figure 4)} and one weaker bond path in *cis-syn,E* (2) {between $H12_{Cy}$ and C_{Ph} (0.0032 e a_0^{-3}; 0.0095 e a_0^{-5}, b4 in Figure 4)}.

The QTAIM results related to the orientation of 2-furyl and the NHCy group in the *Z* and *E* isomers of **1** as discussed above, show that when comparing an intramolecular bond path and bond critical point in *cis-syn,Z* (2) with the related path in *cis-syn,E* (2), the topological parameters (ρ and $\nabla^2\rho$) describing a bond path(s) are in each case stronger for *cis-syn,Z* (2) than for *cis-syn,E* (2).

In summary: the shorter experimental and DFT calculated intramolecular distance N–H· · ·O_{Fu} in *cis-syn,Z* (2), the stronger conjugative LP1(O) → BD*(N–H) NBO calculated interaction and the larger QTAIM calculated electron density and the Laplacian of the electron density at the N–H· · ·O_{Fu} bond critical point in *cis-syn,Z* (2) (conformer 11) compared to the related properties of the C–H· · ·O_{Fu} hydrogen bond in *cis-syn,E* (2) (conformer 12), indicate stabilization of the *Z* configuration of **1**. However, the *cis-syn,E* (2) conformer may also exist since it has similar electronic and Gibbs free energy than *cis-syn,Z* (2) (conformer 11, depending on the computational method) and it also exhibits similar, but slightly weaker NBO interactions and QTAIM calculated bond paths and bond critical points.

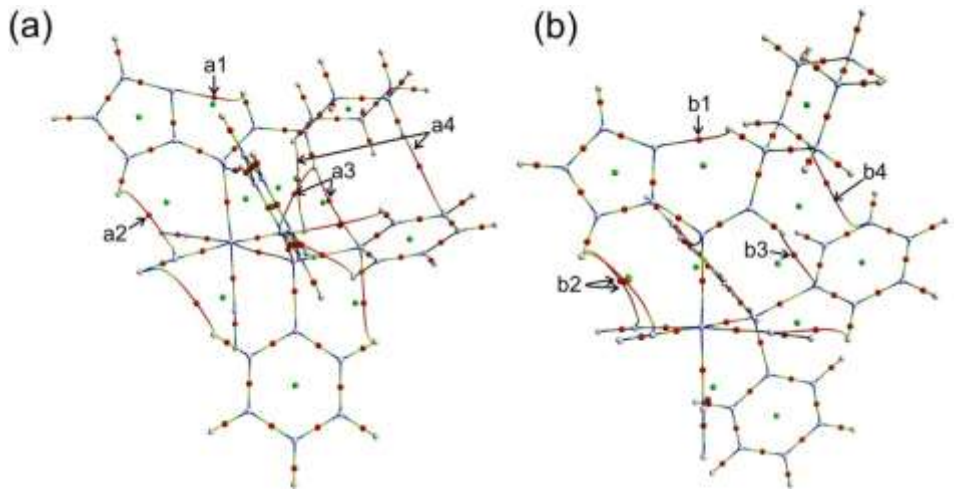

Figure 4. Schematic representation of the critical points (CP) and bond paths (BP) for (a) *cis-syn,Z* (2) and (b) *cis-syn,E* (2). The colour scheme identifying the critical points is as follows; white for (3, −3) or atom critical point; red for (3, −1) or bond CP; green for (3, +1) or ring CP. BPs color scale is according to the value of the electron density: from blue/high to green to red/low. Selected BPs are indicated with small arrows.

Table 5. Topological parameters of the intramolecular hydrogen bonds and the indicated chelate ring in the *cis-syn,Z* (2) and *cis-syn,E* (2) conformers of **1**

	Electron density	Laplacian of the electron density	Eigenvalues of the Hessian matrix		
***cis-syn,Z* (2)**	ρ / e a_0^{-3}	$\nabla^2\rho$ / e a_0^{-5}	λ_1 / e a_0^{-5}	λ_2 / e a_0^{-5}	λ_3 / e a_0^{-5}
Hydrogen bond critical point					
O(Fu)-H(NH)	0.0221	0.1144	-2.44E-02	-1.09E-02	1.50E-01
H(Fu)-C(CO)	0.0089	0.0323	-5.24E-03	-3.70E-03	4.12E-02
H(Cy)-C(CO)	0.0109	0.0332	-8.33E-03	-5.70E-03	4.72E-02
H(Cy)-O(CO)	0.0057	0.0232	-4.27E-03	-2.97E-03	3.04E-02
H(Cy)-C(Ph)	0.0045	0.0144	-3.22E-03	-1.61E-03	1.93E-02
H(Cy)-C(Ph)	0.0041	0.0132	-2.04E-03	-6.40E-04	1.59E-02
H(Ph)-O(CO)	0.0066	0.0253	-5.38E-03	-1.65E-03	3.24E-02
H(Ph)-C(carbene)	0.0089	0.0275	-6.57E-03	-4.71E-03	3.88E-02
H(Ph)-C(Ph)	0.0118	0.0428	-8.42E-03	-3.25E-03	5.44E-02
H(Ph)-C(Ph)	0.0112	0.0413	-8.06E-03	-2.12E-03	5.15E-02
Ring critical point					
5-membered	0.0218	0.1311	-2.15E-02	1.30E-02	1.40E-01
***cis-syn,E* (2)**	r / e a_0^{-3}	$\nabla^2\rho$ / e a_0^{-5}	λ_1 / e a_0^{-5}	λ_2 / e a_0^{-5}	λ_3 / e a_0^{-5}

Hydrogen bond critical point					
O(Fu)-H(Cy)	0.0167	0.07016	-1.67E-02	-1.54E-02	1.02E-01
H(Fu)-C(CO)	0.0074	0.02503	-2.78E-03	-4.65E-04	2.83E-02
H(Fu)-C(CO)	0.0075	0.02571	-2.68E-03	-1.24E-03	2.96E-02
H(Ph)-C(CO)	0.0064	0.02247	-2.72E-03	-1.68E-03	2.69E-02
H(Ph)-C(CO)	0.0071	0.02606	-4.70E-03	-2.13E-03	3.29E-02
H(Cy)-C(Ph)	0.0032	0.00953	-2.17E-03	-1.07E-03	1.28E-02
H(Ph)-C(Carbene)	0.0076	0.02365	-5.05E-03	-2.42E-03	3.11E-02
H(NH)-C(Ph)	0.0050	0.01674	-2.64E-03	-1.88E-03	2.13E-02
Ring critical point					
6-membered	0.0119	0.06896	-6.67E-03	2.19E-02	5.37E-02

4 Conclusions

DFT calculations showed that both the *cis-syn,Z* (2) and *cis-syn,E* (2) conformations of **1** have similar electronic and Gibbs free energies. The shorter experimental and DFT calculated intramolecular distance N–H· · ·O_{Fu} in *cis-syn,Z* (2), the stronger conjugative LP1(O) → BD*(N–H) NBO calculated interaction and the larger QTAIM calculated electron density and the Laplacian of the electron density at the N–H· · ·O_{Fu} bond critical point in *cis-syn,Z* (2) compared to the related properties of the C–H· · ·O_{Fu} hydrogen bond in *cis-syn,E* (2), indicate a higher stabilization of the *Z* configuration of the NHCy group in **1** compared to that of **1**-*E*.

Acknowledgements

This work has received support from the Norwegian Supercomputing Program (NOTUR) through a grant of computer time (Grant No. NN4654K) (JC), the South African National Research Foundation (JC, ML), HPC Warehouse Facility and the Central Research Fund of the University of the Free State, Bloemfontein (JC) and the University of Pretoria (ML).

Supporting Information

The electronic supporting information includes Table S1, lists of bond distances and angles for crystal structures reported and the optimized coordinates of the DFT calculations. CCDC 1048219 contains the supplementary crystallographic data for this paper. These data can be obtained free of charge via http://www.ccdc.cam.ac.uk/conts/retrieving.html (or from the Cambridge Crystallographic Data Centre, 12, Union Road, Cambridge CB2 1EZ, UK; fax: +44 1223 336033).

References

[1] E.O. Fischer, A. Maasböl, Angew. Chem. 76 (1964) 645.

[2] (a) L.S. Hegedus in: E.W. Abel, F.G.A. Stone, G. Wilkinson (Eds.), Comprehensive Organometallic Chemistry II, Pergamon Press, Oxford, UK, 1995, Vol.12, p 549. (b) W.D. Wulff in: B.M. Trost, I. Fleming (Eds.), Comprehensive Organic Synthesis, Pergamon Press, Oxford, UK, 1991, Vol.5, p 65. (c) W.D. Wulff, in: E.W. Abel, F.G.A. Stone, G. Wilkinson (Eds.), Comprehensive Organometallic Chemistry II, Pergamon Press, Oxford, UK, 1995, Vol.12, p 469.

[3] (a) M. L. Waters, T.A. Brandvold, L. Isaacs, W.D. Wulff, Organometallics 17 (1998) 4298. (b) D. K. Sinha-Mahapatra, D. Hazra, V. G. Puranik, A. Sarkar, J. Organomet. Chem. 689 (2004) 3501. (c) L. Vyklicky, H. Dvořáková, D. Dvořák, Organometallics 20 (2001) 5419.

[4] J. Barluenga, K. Muñiz, A. Ballesteros, S. Martínez, M. Tomás, ARKIVOC (2002) 110.

[5] (a) M. Brookhart, W.B. Studabaker, Chem. Rev., 87 (1987), 411. (b) D.F. Harvey, D.M. Sigano, Chem. Rev. 96 (1996) 271.

[6] E. Moser, E.O. Fischer, J. Organomet. Chem. 16 (1969) 275.

[7] (a) A. Hafner, L.S. Hegedus, G. de Weck, B. Hawkins, K.H. Dötz, J. Chem. Soc. 110 (1988) 8413 (b) D.J. Cardin, B. Cetinkaya, M.F. Lappert, Chem. Rev. 72 (1972) 545. (c) M.Y. Darensbourg, D. Darensbourg, J. Inorg. Chem. 9 (1970) 32.

[8] E. Licandro, S. Maiorana, D. Perdicchia, C. Baldoli, C. Graiff, A. Tiripicchio, J. Organomet. Chem. 617–618 (2001) 399.

[9] M. Landman, T.J. Levell, M.M. Conradie, P.H. van Rooyen, J.Conradie, J. Mol. Struct. 1086 (2015) 190.

[10] D.F. Schriver, M.A. Drezdzon, The manipulation of Air-Sensitive Compounds, 2nd ed., Wiley, New York, USA, 1986.

[11] H. Meerwein, Org. Synth. 46 (1966) 113.

[12] J.P. Perdew, J.A. Chevary, S.H. Vosko, K.A. Jackson, M.R. Pederson, D.J. Singh and C. Fiolhais, Phys. Rev. B, 46 (1992) 6671-6687. Erratum: J.P. Perdew, J.A. Chevary, S.H. Vosko, K.A. Jackson, M.R. Perderson, D.J. Singh and C. Fiolhais, Phys. Rev. B, 48 (1993) 4978.
[13] A.D. Becke, Phys. Rev. A 38 (1988) 3098.
[14] C.T. Lee, W.T. Yang, R.G. Parr, Phys. Rev. B 37 (1988) 785.
[15] Y. Zhao and D.G. Truh, Acc. Chem. Res. 41 (2008) 147.
[16] M.J. Frisch, G.W. Trucks, H.B. Schlegel, G.E. Scuseria, M.A. Robb, J.R. Cheeseman, G. Scalmani, V. Barone, B. Mennucci, G.A. Petersson, H. Nakatsuji, M. Caricato, X. Li, H.P. Hratchian, A.F. Izmaylov, J. Bloino, G. Zheng, J.L. Sonnenberg, M. Hada, M. Ehara, K. Toyota, R. Fukuda, J. Hasegawa, M. Ishida, T. Nakajima, Y. Honda, O. Kitao, H. Nakai, T. Vreven, J.A. Montgomery (Jr), J.E. Peralta, F. Ogliaro, M. Bearpark, J.J. Heyd, E. Brothers, K.N. Kudin, V.N. Staroverov, T. Keith, R. Kobayashi, J. Normand, K. Raghavachari, A. Rendell, J.C. Burant, S.S. Iyengar, J. Tomasi, M. Cossi, N. Rega, J.M. Millam, M. Klene, J.E. Knox, J.B. Cross, V. Bakken, C. Adamo, J. Jaramillo, R. Gomperts, R.E. Stratmann, O. Yazyev, A.J. Austin, R. Cammi, C. Pomelli, J.W. Ochterski, R.L. Martin, K. Morokuma, V.G. Zakrzewski, G.A. Voth, P. Salvador, J.J. Dannenberg, S. Dapprich, A.D. Daniels, O. Farkas, J.B. Foresman, J.V. Ortiz, J. Cioslowski, D.J. Fox, Gaussian 09, Revision D.01, Gaussian Inc., Wallingford CT, 2010.
[17] F. Weigend, R. Ahlrichs, Phys. Chem. Chem. Phys. 7 (2005) 3297.
[18] E.D. Glendening, J.K. Badenhoop, A.E. Reed, J.E. Carpenter, J.A. Bohmann, C.M. Morales, and F. Weinhold, NBO 3.1 (Theoretical Chemistry Institute, University of Wisconsin, Madison, WI, USA, 2001).
[19] (a) R.F.W. Bader, Chem. Rev. 91 (1991) 893. (b) F. Cortés-Guzmán, R.F.W. Bader, Chem. Rev. 249 (2005) 633.
[20] J.I. Rodríguez, R.F.W. Bader, P.W. Ayers, C. Michel, A.W. Götz and C. Bo, A high performance grid-based algorithm for computing QTAIM properties. Chemical Physics Letters 472 (2009) 149.
[21] (a). G. te Velde, F.M. Bickelhaupt, S.J.A. van Gisbergen, C. Fonseca Guerra, E.J. Baerends, J.G. Snijders and T. Ziegler, . J. Compt. Chem. 22 (2001) 93.1 (b) C. Fonseca Guerra, J.G. Snijders, G. te Velde and E.J. Baerends, Theoretical Chemistry Accounts 99 (1998) 391 . (c) ADF2013, SCM, Theoretical Chemistry, Vrije Universiteit, Amsterdam, The Netherlands, http://www.scm.com.
[22] APEX2 (including SAINT and SADABS); Bruker AXS Inc., Madison, WI, 2012.
[23] G.M. Sheldrick, Acta Crystallogr. A 64 (2008) 112.
[24] L.J.J. Faruggia, Appl. Crystallogr. 30 (1997) 565.
[25] (a) H. Werner, H. Rascher, Inorg. Chim. Acta 2 (1968) 181. (b) E.O. Fischer, R. Aumann, Chem. Ber. 102 (1969) 1495. (c) J. Barluenga, K. Muniz, M. Tomas, A. Ballesteros, S. Garcia - Granda, Organometallics 22 (2003) 1756. (d) A. Arrieta, F.P. Cossío, I. Fernández, M. Gomez-Gallego, B. Lecea, M.J. Mancheno, M.A. Sierra, J. Am. Chem. Soc. 122 (2000) 11509. (e) M.D. Cooke, E.O. Fischer, J. Organomet. Chem. 56 (1973**)** 279. (f) E.O. Fischer, H. Fischer, Chem. Ber. 107 (1974) 657. (g) R. Streubel, S. Priemer, P.G. Jones, J. Organomet. Chem. 618 (2001) 423.

[26] M Landman, R. Pretorius, R. Fraser, B.E. Buitendach, M.M. Conradie, P.H. van Rooyen, J. Conradie, Electrochim. Acta 130 (2014) 104.

[27] M. Landman, T. Levell, P.H. van Rooyen, J. Conradie, J. Mol. Struct. 1065–1066 (2014) 29.

[28] (a) B. Heckl, H. Werner, E.O. Fischer, Angew. Chem. Int. Ed. Engl. 7 (1968) 817. (b) C.F. Bernasconi, M.W. Stronach, J. Am. Chem. Soc. 115 (1993) 1341. (c) R. Imwinkelried, L.S. Hegedus, Organometallics 7 (1988) 702.

[29] Cambridge Structural Database (CSD), Version 5.35, May 2014 update, CSD reference codes: FIPNIB, GOFXOP, JELGEN, JELGIR, MEJLAO, QESYOC, QESYUI, WEXMUI, ZAFWEI, CIWRIL, CIWROR, CIWRUX

[30] (a) S. Thompson, H.R. Wessels, R. Fraser, P.H. van Rooyen, D.C. Liles, M. Landman, J. Mol. Struct. 1060 (2014) 111. (b) M. Landman, R. Liu, R. Fraser, P.H. van Rooyen, J. Conradie, J. Organomet. Chem. 752 (2014) 171. (c) D.I. Bezuidenhout, D.C. Liles, P.H. van Rooyen, S. Lotz, J. Organomet. Chem. 692, (2007), 774.

[31] M. Landman, R. Pretorius, B.E. Buitendach, P.H. van Rooyen, J. Conradie, Organometallics, 32 (2013) 5491.

[32] T, Ziegler, Can. J. Chem. 73 (1995) 743.

[33] G.A. Jeffrey, An introduction to hydrogen bonding, Oxford University Press, 1997, p.12.

[34] H. Szatyłowicz, J. Phys. Org. Chem. 21 (2008) 897.

[35] G.R. Desira, Acc. Chem. Res. 24 (1991) 290.

[36] A. Bondi, J. Phys. Chem. 68 (1964) 441.

[37] R.F.W. Bader, J. Phys. Chem. A (1998) 102.